Journal of Sound and Vibration (1998) **217**(1), 113–126
Article No. sv981729

THE CONTRIBUTION OF RADIATION AND VISCOUS LOSS IN A FLUID LOADED FLEXURAL PLATE WAVE SENSOR

J. L. DOHNER

Sandia National Laboratories, Department 9234, *MS* 0439, *P.O. Box* 5800, *Albuquerque, NM* 87185-0439, *U.S.A.*

(*Received* 10 *October* 1997, *and in final form* 5 *May* 1998)

In this paper a study of radiation and viscous losses in a fluid loaded Flexural Plate Wave (FPW) sensor is presented. Previous to this study, it was believed that supersonic radiation was the dominant mechanism of damping in FPW devices. However, because no previous theory had been developed to model finite length effects, this belief was never challenged. In this paper it will be shown that the dominant mechanism of damping can not only be due to supersonic radiation, but also to a fluid/structure resonance which enhances viscous loss. The equations of motion for a single port FPW sensor plate are derived and coupled to the equations of motion for a Newtonian fluid. These coupled equations are solved by using a wave number transform approach. The resulting solution is comprised of terms derived by Wenzel, plus additional terms representing diffracted wave dynamics. It is shown that significant viscous damping occurs when a resonance involving diffracted wave dynamics is excited.

© 1998 Academic Press

1. INTRODUCTION

In the macro-domain, structural coupling to many fluids such as air is weak and relaxation effects are minimal; therefore, these fluids can usually be modelled as light fluids with little loss. However, as the size of the structure is reduced and as the frequency of excitation is increased, many of these fluids can no longer be modelled as a light and lossless. At small scales and high frequencies, shear wave propagation becomes significant, and fluids such as air must be modelled as heavy, viscous, heat conducting fluids. For many problems this makes the analysis and prediction of fluid damping in MicroElectroMechanical devices (MEMs) more difficult than the analysis and prediction of fluid damping in similar, larger, macro-domain devices. In this paper the authors attempt to understand some of the mechanisms which cause damping in a specific MEMs sensor. Traditionally it was believed that the mechanisms which produce damping limit performance in the macro-domain where the same mechanisms which produce damping and limit performance in the micro-domain, but as will be shown, in the micro-domain, other mechanisms can also play a significant role in mitigating the response of the structure.

0022–460X/98/410113 + 14 $30.00/0 © 1998 Academic Press

In fluid loaded MEMs devices, damping occurs due to energy losses in the structure or due to energy losses into the fluid. Nevertheless, in Flexural Plate Wave (FPW) sensors [1], structural damping is usually small [2] and most energy is lost into the fluid. Losses into the fluid can be due to relaxation effects such as those caused by viscosity and heat transfer, or can be due to radiation effects such as those due to edge diffraction. In this paper, a study of damping loss due to viscous relaxation and radiation is presented for a FPW sensor.

Viscous relaxation occurs in a number of different processes. Two well studied processes are small amplitude fluid motion around a structure and squeeze [3]. The first process is similar to that which is found in a micro-tuning fork. After excitation the tuning fork slowly loses energy via irreversible viscous air motion around its prongs. This process can be represented by a lossy non-propagating wave solution. Kokubun *et al*. [4] developed a ''string of beads'' model to represent this process, and Hosaka *et al*. [2] used Kokubun's model with a squeeze model to model the dynamics of a micro-beam. Other researchers have also expanded upon Kokubun's work to approximate damping due to this process [5]. Another form of damping is radiation damping. Radiation damping is due to propagating waves which transport energy into the far field. Cho *et al*. [6] developed a model for the fluid damping of a micro comb drive using a shear wave solution. Although sufficient for the prediction of damping in a comb drive, their model did not include radiation effects since the waves in their model were non-propagating. Their model was an improvement over a simpler Couette-type (non-wave) model.

Wenzel [7] and Martin *et al*. [8] developed a more complex, non-propagating, wave model for viscous damping in FPW sensors. Although derived for non-propagating waves, this model could be used to represent damping due to radiation by allowing wave numbers to be complex. Nevertheless, Wenzel assumed that plate dimensionality was infinite, and therefore, resonances due to edge diffraction were neglected. These resonance effects can enhance viscous relaxation in the fluid which, in return, produces a high amount of damping on the structure. In this paper the Wenzel solution will be extended to include these neglected effects. It will be shown that resonances due to diffracted wave dynamics can have a catastrophic effect on sensor performance.

2. DERIVATION OF EQUATIONS OF MOTION

A single port, Lorentz actuated FPW sensor [8] is illustrated in Figure 1. This sensor consists of a thin SiN plate/membrane with a serpentine layer of gold wire laid back and forth across its length. The SiN plate/membrane is supported by a Si base which produces a clamped boundary condition at its edges. The effect of the serpentine layer of gold is to spatially couple electrical excitations and responses of the sensor to a single mechanical mode. Therefore, the electrical dynamics of the FPW sensor look like a simple second order, resonant system. Species selective coatings are applied across the surface of the SiN membrane for the purpose of absorbing mass from the surrounding fluid, thereby increasing the mass of the membrane relative to the concentration of species in the surrounding fluid and altering the natural frequency of the spatially filtered mode. Since the

natural frequency of this mode can be correlated with the concentration of species in the surrounding fluid, this device can be used as a sensor to measure species concentrations in a fluid. To measure the natural frequency of the spatially filtered mode, the electrical impedance of this sensor must be measured. To measure this electrical impedance, the sensor is electrically excited by a Lorentz force resulting from the interaction of a supplied current, i, with a supplied constant magnetic field, B. The response of the electrical system is measured by a voltmeter across the wire; thereby, the impedance of the electrical side of the system can be deduced. This impedance response will be second order with a natural frequency dependent on the concentration of species in the surrounding fluid.

Damping in the electrical side of the system is a function of the damping in the spatially filtered mechanical mode. If this damping is very small, then the natural frequency of the electrical system is easily identified by measuring the frequency at which the impedance magnitude peaks; however, if this damping is large, then no peak occurs, and the natural frequency cannot be easily identified. If simple methods are used to identify the natural frequency of the electrical system, then too much damping will make the device non-functional.

Damping in a FPW device is due to relaxation and radiation in the fluid. In the past it was believed that significant damping occurred in these devices due to supersonic radiation effects. This belief was derived from macro-domain theory and from the fact that at coincidence, the FPW device is non-functional. In the following work, the present theory has been expanded to explore the validity of this believe.

Assuming that the length of the SiN plate is long compared to its width and that the excited mode is comprised of waves with low wave numbers in the length direction, a two-dimensional analysis of Figure 1 sensor is appropriate. Moreover, for high wave numbers in the width direction, a simply supported boundary condition can be assumed. In this paper, less then 7% error in the natural frequency of the excited mode occurs due to this assumption.

Using the above assumptions, the complex three-dimensional Figure 1 system can be approximated by a less complex, two-dimensional Figure 2 system. The

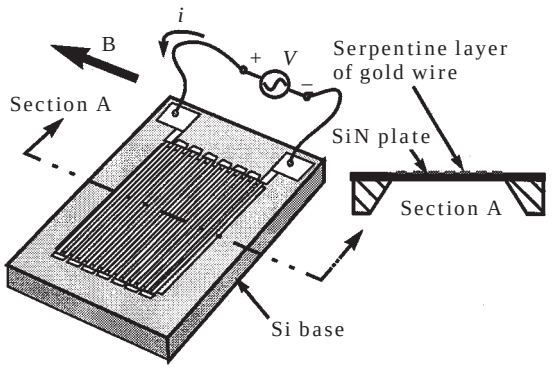

Figure 1. An illustration of a single port flexural plate wave sensor.

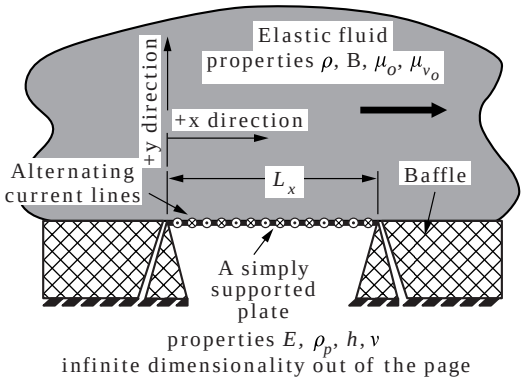

Figure 2. A two-dimensional approximation of the single port sensor.

dynamics of this two-dimensional approximation can be solved in closed form, thereby, supplying greater insight into relevant physics.

In the simplified system, the plate is h thick, L_x long, and is comprised of a SiN linear elastic material with elastic modulus, E, Poisons ratio, v, and density, ρ_p. The plate contains a tensile force per unit length, T. A differential element of the plate can move with x and y displacement, $u_x(x)$ and $u_y(x)$. Current lines run back and forth across the infinite length of the plate. Current, i, interacting with a supplied magnetic field, B, produces a Lorentz force excitation on the plate. Current is driven by a voltage per unit length, V. A semi-infinite linear Newtonian fluid with bulk modulus, B, shear viscosity, μ_o, bulk viscosity, μ_{v_o}, and density, ρ, loads the plate.

A differential element of the plate is shown in Figure 3. The shear force in the plate is V_x, the moment in the plate is M_x, the rotation of the plate is θ, the fluid shear stress on the plate is τ_{xy}, and the normal stress on the plate is τ_{yy}. Summing forces in the y direction gives

$$\frac{\partial V_x}{\partial x} + T\frac{\partial \theta}{\partial x} + \theta\frac{\partial T}{\partial x} - \tau_{yy} = \rho_p h\frac{\partial^2 u_y}{\partial t^2}. \tag{1}$$

Summing the moments gives

$$V_x = \frac{\partial M_x}{\partial x} - \frac{h}{2}\tau_{xy}. \tag{2}$$

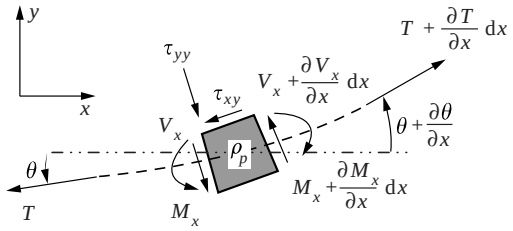

Figure 3. A differential element of the plate of the single port sensor.

Combining equations (1) and (2) and noting that $\theta = \partial u_y/\partial x$ gives the non-linear equation of motion for the plate,

$$\frac{\partial^2 M_x}{\partial x^2} - \frac{h}{2}\frac{\partial \tau_{xy}}{\partial x} - \tau_{yy} + T \cdot \frac{\partial^2 u_y}{\partial x^2} + \frac{\partial u_y}{\partial x} \cdot \frac{\partial T}{\partial x} = \rho_p h \frac{\partial^2 u_y}{\partial t^2}. \tag{3}$$

The linearized equation of motion can be determined by perturbation analysis where $u_y = u_{y_1}\varepsilon$, $T = T_o + T_1\varepsilon$, $M_x = M_{x_1}\varepsilon$, $\tau_{xy} = \tau_{xy_1}\varepsilon$, $\tau_{yy} = \tau_{yy_1}\varepsilon$, and ε is a small value. Substituting these equations into equation (3) and collecting ε order terms gives

$$\frac{\partial^2 M_{x_1}}{\partial x^2} + T_o \frac{\partial^2 u_{y_1}}{\partial x^2} - \rho_p h \frac{\partial^2 u_{y_1}}{\partial t^2} = \frac{h}{2}\frac{\partial \tau_{xy_1}}{\partial x} + \tau_{yy}. \tag{4}$$

Using classical analysis [9, 10], the moment, M_{x_1}, is related to the normal displacement as

$$M_{x_1} = -D\frac{\partial^2 u_{y_1}}{\partial x^2}, \tag{5}$$

where $D = Eh^3/12(1 - \nu^2)$. Substituting equation (4) into equation (5) and taking the temporal Fourier transform gives

$$\left(\frac{D}{\rho_p h}\frac{\partial^2}{\partial x^2} - \frac{T_o}{\rho_p h}\right) \cdot \frac{\partial^2 u_{y_1}}{\partial x^2} - \omega^2 \frac{\partial^2 u_{y_1}}{\partial t^2} = \frac{-1}{\rho_p h}\left(\tilde{\tau}_{yy_1} + \frac{h}{2}\frac{\partial \tilde{t}_{xy_1}}{\partial x}\right), \tag{6}$$

where $\tilde{x} = \int_{-\infty}^{\infty} x\, e^{j\omega t}\, dt$, $j = \sqrt{-1}$, and ω is a circular frequency.

Equation (6) is the linear equation of motion of an *in vacuo* plate drive by an external normal and shear stress. This equation was derived here to show the inclusion of the shear stress excitation τ_{xy} which is usually neglected in most plate analyses [9, 10] but is necessary to couple the dynamics of the plate/membrane to the dynamics of the fluid.

The normal stress can be expressed in terms of a stress due to the fluid and a stress due to the Lorentz force excitation as

$$\tilde{\tau}_{yy_1} = -iB\sum_{k=1}^{14}(-1)^{k-1}\delta\left(x - \frac{2k-1}{28}L_x\right) + \tilde{\tau}_{yy_{1_f}}, \tag{7}$$

where $\tilde{\tau}_{yy_{1_f}}$ is the normal stress on the plate due to the fluid and $\delta(x)$ is a Dirac delta function.

Combining equation (7) with equation (6) and decomposing the result into *in vacuo* modes gives

$$a_m\left(\frac{\tilde{A}_m}{i}\right) = b_m - \frac{1}{\rho_p h}\int_0^{L_x} \frac{\tilde{g}(x)}{i}\sin\left(\frac{m\pi}{L_x}x\right)dx, \tag{8}$$

where

$$a_m = \frac{L_x}{2}(\omega_m^2 - \omega^2), \qquad \omega_m^2 = \left(\frac{D}{\rho_p h}\left(\frac{m\pi}{L_x}\right)^2 + \frac{T_o}{\rho_p h}\right)\left(\frac{m\pi}{L_x}\right)^2,$$

$$\tilde{u}_{y_1} = \sum_{m=1}^{\infty} \tilde{A}_m \sin\left(\frac{m\pi}{L_x} x\right),$$

$$b_m = \frac{B}{\rho_p h} \sum_{k=1}^{14} -1^{k-1} \sin\left(m\pi \frac{(2k-1)}{28}\right), \qquad \tilde{g}(x) = \tilde{\tau}_{yy_{1_f}} + \frac{h}{2}\frac{\partial \tilde{\tau}_{xy_1}}{\partial x}.$$

Equation (8) is a modal representation of plate dynamics. In the following section, the function $\tilde{g}(x)$ will be represented in terms of these same modes.

From Temkin [11], the linearized displacement of the fluid can be represented as

$$\tilde{u}_{x_1}\hat{\mathbf{i}} + \tilde{u}_{y_1}\hat{\mathbf{j}} = \nabla\tilde{\phi} + \nabla \times \tilde{\psi}, \tag{9}$$

where $\tilde{u}_{x_1}$ and $\tilde{u}_{y_1}$ are the x and y displacements of a fluid particle, $\hat{\mathbf{i}}$ and $\hat{\mathbf{j}}$ are x and y direction unit vectors, and $\tilde{\phi}$ and $\tilde{\psi}$ are potential functions where

$$(\nabla^2 + k_l^2)\tilde{\phi} = 0, \qquad (\nabla^2 + k_s^2)\tilde{\psi} = 0, \tag{10, 11}$$

$$k_l^2 = \frac{\omega^2/c_o^2}{1 - \mathrm{j}\omega(4\nu_o'/3c_o^2)} = \frac{\omega^2}{c_l^2}, \qquad k_s^2 = \frac{\omega^2}{-\mathrm{j}\omega\nu_o} = \frac{\omega^2}{c_s^2}, \tag{12, 13}$$

where $c_o^2 = B/\rho$ is the acoustic sound speed, $\nu_o' = 1/\rho(\mu_o + \frac{3}{4}\mu_{\nu_o})$, and $\nu_o = \mu_o/\rho$ is the specific viscosity. In air, Temkin used the work of Greenspan [12], to approximate the bulk viscosity of air as $\mu_{\nu_o} \approx 0{\cdot}65\mu_o$. Using the fact that $c_l^2 = (\lambda + 2\mu)/\rho$ and that $c_s^2 = \mu/\rho$ [13], $\mu = -\mathrm{j}\omega\mu_o$ and $\lambda = \mathrm{B} - \mathrm{j}\omega(\mu_{\nu_o} - \frac{2}{3}\mu_o)$.

Equations (9), (10) and (11) are the equations of motion for the fluid. These equations are coupled to the equations of motion of the plate by the stress displacement relations

$$\tilde{\tau}_{yy_1} = (\lambda + 2\mu)\left\{\frac{\partial \tilde{u}_{y_1}}{\partial y} + \frac{\partial \tilde{u}_{x_1}}{\partial x}\right\} - 2\mu\frac{\partial \tilde{u}_{x_1}}{\partial x}, \qquad \tilde{\tau}_{xy_1} = 2\mu\left\{\frac{\partial \tilde{u}_{x_1}}{\partial y} + \frac{\partial \tilde{u}_{y_1}}{\partial x}\right\}, \tag{14, 15}$$

and the potential displacement relations

$$\mu_{x_1} = \frac{\partial}{\partial x}\tilde{\phi} + \frac{\partial}{\partial y}\tilde{\psi}, \qquad u_{y_1} = \frac{\partial}{\partial y}\tilde{\phi} - \frac{\partial}{\partial x}\tilde{\psi}, \tag{16, 17}$$

evaluated at $y = 0$.

3. SOLUTION OF THE EQUATIONS OF MOTION

The equations of motion (6), (9–11) are solved by using a wave transform approach. By definition, the wave number transform of ϕ is

$$\tilde{\Phi}(\gamma) = \int_{-\infty}^{\infty} \tilde{\phi}(x)\, \mathrm{e}^{-\mathrm{j}\gamma x}\, \mathrm{d}x. \tag{18}$$

In the wave number domain, the solution to equations (10) and (11) can be written as

$$\tilde{\Phi} = A\, \mathrm{e}^{\mathrm{j}qy} \quad \text{and} \quad \tilde{\Psi} = B\, \mathrm{e}^{\mathrm{j}sy}, \tag{19, 20}$$

where $\tilde{\Psi}(\gamma)$ is the wave number transform of $\tilde{\Psi}(x)$, $q = \sqrt{k_l^2 - \gamma^2}$ and $s = \sqrt{k_s^2 - \gamma^2}$. Following the derivation by Wenzel [7], taking the transform of equations (3c, d) making the assumption that $\tilde{u}_x(x, y = 0) \cong h/2(\partial/\partial x)\tilde{u}_y(x, y = 0)$‡ and solving for A and B gives

$$A = \frac{\mathrm{j}s + \mathrm{j}\gamma r}{\gamma^2 + qs}, \qquad B = \frac{\mathrm{j}qr - \mathrm{j}\gamma}{\gamma^2 + qs}, \tag{21, 22}$$

where $r = -\mathrm{j}\gamma(h/2)$. Substituting equations (21) and (22) into equations (19) and (20), the result into the wave number transform of equations (16) and (17), that result in equations (14) and (15), that result in the wave number transform for the expression for $g(\tilde{x})$, simplifying and neglecting small terms gives

$$\frac{\tilde{G}(\gamma)}{\tilde{U}_y(\gamma, y = 0)} = \mathrm{j}\omega^2\rho\, \frac{s}{\gamma^2 + sq}, \tag{23}$$

where $\tilde{G}(\gamma)$ is the wave number transform of $\tilde{g}(x)$ and $\tilde{U}_y(\gamma)$ is the wave number transform of $\tilde{u}_y(x)$.

Since $\tilde{u}_y(x, y = 0)$ can be expressed in terms of the *in vacuo* modes of the plate and the wave number transform is a linear operator, $\tilde{U}_y(\gamma, y = 0)$ can be expressed in terms of the wave number transform of the *in vacuo* modes of the plate. Representing $\tilde{U}_y(\gamma, y = 0)$ in terms of *in vacuo* modes, solving for $\tilde{G}(\gamma)$ and inverse transforming gives

$$\tilde{g}(x) = -\mathrm{j}\frac{\omega^2\rho}{2\pi} \sum_{n=1}^{\infty} \tilde{A}_n[\tilde{I}_1(n, x) - (-1)^n \tilde{I}_1(n, x - L_x)], \tag{24}$$

where

$$\tilde{I}_1(n, x) = \int_{-\infty}^{\infty} \frac{\dfrac{n\pi}{L_x}\sqrt{k_s^2 - \gamma^2}\, \mathrm{e}^{-\mathrm{j}\gamma x}}{\left(\left(\dfrac{n\pi}{L_x}\right)^2 - \gamma^2\right)(\gamma^2 + \sqrt{k_s^2 - \gamma^2}\sqrt{k_l^2 - \gamma^2})}\, \mathrm{d}\gamma.$$

‡ This assumption comes from the derivation of flexural wave motion in an unloaded plate.

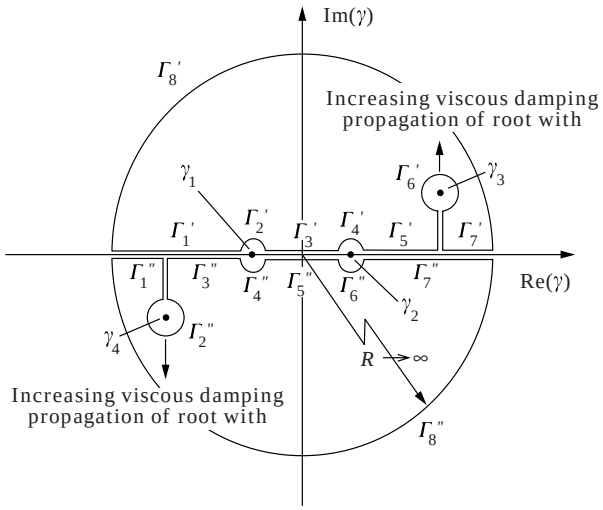

Figure 4. Contour integration used to calculate $\tilde{I}_1(n, x)$.

$\tilde{I}_1(n, x)$ can be solved by using a contour integration. The poles of the integrand of $I_1(n, x)$ are $\gamma_1 = n\pi/L_x$, $\gamma_2 = n\pi/L_x$, $\gamma_3 = -\sqrt{k_s^2 k_l^2/(k_s^2 + k_l^2)}$ and $\gamma_4 = \sqrt{[k_s^2 k_l^2/(k_s^2 + k_l^2)]}$, and the branch integrations are shown in Figure 4. The integral, $\tilde{I}_1(n, x)$, can be determined from a contour integration over the upper or lower half of the γ plane. The use of the upper or lower half is dependent upon the convergence of the Γ_8' and Γ_8'' branches. Computing the integral of the $\tilde{I}_1(n, x)$ integrandover the Γ_8' branch, letting $\gamma = \lim_{R\to\infty} \mathrm{Re}^{i\theta}$, and noting that $\lim_{R\to\infty}(R^2 \mathrm{e}^{i2\theta} + \sqrt{k_s^2 - R^2 \mathrm{e}^{i2\theta}}\sqrt{k_l^2 - R^2 \mathrm{e}^{i2\theta}}) = (k_s^2 + k_l^2)/2$, gives

$$\lim_{R\to\infty} \int_0^{\pi} \frac{\dfrac{n\pi}{L_x}\sqrt{k_s^2 - R^2 \mathrm{e}^{i2\theta}}\, \mathrm{e}^{-\mathrm{j}xR\cos\theta}\, \mathrm{e}^{xR\sin\theta}}{\left(\left(\dfrac{n\pi}{L_x}\right)^2 - R^2 \mathrm{e}^{i2\theta}\right)(R^2 \mathrm{e}^{i2\theta} + \sqrt{k_s^2 - R^2 \mathrm{e}^{i2\theta}}\sqrt{k_l^2 - R^2 \mathrm{e}^{i2\theta}})}$$

$$Ri\, \mathrm{e}^{i\theta}\, \mathrm{d}\theta \to \begin{cases} \infty & \text{for} \quad x > 0, \\ 0 & \text{for} \quad x < 0. \end{cases}$$

Computing the integral over the Γ_8'' branch gives

$$\lim_{R\to\infty} \int_{\pi}^{2\pi} \frac{\dfrac{n\pi}{L_x}\sqrt{k_s^2 - R^2 \mathrm{e}^{i2\theta}}\, \mathrm{e}^{-\mathrm{j}xR\cos\theta}\, \mathrm{e}^{xR\sin\theta}}{\left(\left(\dfrac{n\pi}{L_x}\right)^2 - R^2 \mathrm{e}^{i2\theta}\right)(R^2 \mathrm{e}^{i2\theta} + \sqrt{k_s^2 - R^2 \mathrm{e}^{i2\theta}}\sqrt{k_l^2 - R^2 \mathrm{e}^{i2\theta}})}$$

$$Ri\, \mathrm{e}^{i\theta}\, \mathrm{d}\theta \to \begin{cases} 0 & \text{for} \quad x > 0, \\ \infty & \text{for} \quad x < 0. \end{cases}$$

Therefore, the lower set of branches can be used to evaluate $\tilde{I}_1(n, x)$ for $x > 0$ and the upper set of branches can be used to evaluate $\tilde{I}_1(n, x)$ for $x < 0$. The integration around other branches is calculated using standard techniques [14]. Substituting the result for $\tilde{I}_1(n, x)$ into equation (24) gives

$$\tilde{g}(x) = \sum_{n=1}^{\infty} \tilde{A}_n \left\{ \left\{ \begin{array}{cc} C_1(n) \sin\left(\dfrac{n\pi}{L_x} x\right) & \text{for } 0 < x < L_x \\ 0 & \text{otherwise} \end{array} \right\} \right.$$

$$\left. + \left\{ \begin{array}{cc} C_2(n)\, \mathrm{e}^{-\mathrm{j}\sqrt{k_s^2 k_l^2/k_s^2 + k_l^2}\, x} & \text{for } x > 0 \\ C_2(n)\, \mathrm{e}^{\mathrm{j}\sqrt{k_s^2 k_l^2/k_s^2 + k_l^2}\, x} & \text{for } x < 0 \\ -(-1)^n C_2(n)\, \mathrm{e}^{-\mathrm{j}\sqrt{k_s^2 k_l^2/k_s^2 + k_l^2}(x - L_x)} & \text{for } x > L_x \\ -(-1)^n C_2(n)\, \mathrm{e}^{\mathrm{j}\sqrt{k_s^2 k_l^2/k_s^2 + k_l^2}(x - L_x)} & \text{for } x < L_x \end{array} \right\} \right\}, \quad (25)$$

where

$$C_1(n) = \frac{\mathrm{j}\omega^2 \rho \sqrt{k_s^2 - \left(\dfrac{n\pi}{L_x}\right)^2}}{\left(\dfrac{n\pi}{L_x}\right)^2 - \sqrt{k_l^2 - \left(\dfrac{n\pi}{L_x}\right)^2} \sqrt{k_s^2 - \left(\dfrac{n\pi}{L_x}\right)^2}} \quad \text{and}$$

$$C_2(n) = \frac{-\omega^2 \rho \dfrac{n\pi}{L_x} \dfrac{k_s^2}{\sqrt{k_s^2 + k_l^2}}}{\left(\left(\dfrac{n\pi}{L_x}\right)^2 - \dfrac{k_s^2 k_l^2}{k_s^2 + k_l^2}\right)(k_s^2 + k_l^2) \sqrt{\dfrac{k_s^2 + k_l^2}{k_s^2 k_l^2}}}.$$

The bracketed expression in equation (25) is the solution for the force on the plate due to the excitation of the n^{th} *in vacuo* mode. Note that the first term in brackets is the result of Wenzel. The second set of terms in brackets is due to edge diffraction.

Substituting equation (25) into equation (8) gives

$$a_m\left(\frac{\tilde{A}_m}{i}\right) = b_m + \sum_{n=1}^{\infty} c_{mn}\left(\frac{\tilde{A}_n}{i}\right), \quad (26)$$

where

$$c_{mn} = -\frac{1}{\rho_p h} \quad C_1(n) \frac{L_x}{2} \delta_{mn} - C_2(n) \frac{\dfrac{m\pi}{L_x}}{\left(\dfrac{m\pi}{L_x}\right)^2 - \dfrac{k_s^2 k_l^2}{k_s^2 + k_l^2}}$$

$$\left\{1 + (-1)^{m+n} - ((-1)^n + (-1)^m)\, \mathrm{e}^{-\mathrm{j}k_s^2 k_l^2/k_s^2 + k_l^2 L_x}\right\} \quad . \quad (27)$$

A matrix solution can be used to solve equation (26) for $\tilde{A}_m$ where $m = 1, 2, 3 \ldots$. This solution can then be used to solve for the impedance of the electrical system,

$$\frac{V}{i} = R - j\omega B \sum_{l=1}^{14} \sum_{m=1}^{\infty} \left(\frac{\tilde{A}_m}{i} \right) \sin \left(\frac{2l-1}{28} L_x \right) (-1)^{l-1}. \tag{28}$$

4. NUMERICAL RESULTS

In this section the equations of motion will be solved for an air loaded SiN plate. The properties of the plate and air are given in Table 1. The tension in the plate was adjusted such that the spatially filtered, excited mode always had a natural frequency of 0·406 MHz.

To study the mechanisms by which the plate loses energy to the fluid, the length of the plate was varied. As the length of the plate was varied, the sound speed of waves in the plate/membrane was altered by an associated variation in tension. Sound speeds in the plate were subsonic, supersonic, or sonic to waves in the fluid. In this problem the major damping mechanism in the plate was due to a resonance in both the fluid and the structure. This resonance occurred when the waves in the plate were sonic to diffracted waves in the fluid.

This resonance can be seen in equation (25). The first term in the outer brackets of this equation is the forced excitation response. Note that the C_1 coefficient in front of this term is Wenzel's expression for fluid loading. The second set for terms represents loading due to edge diffraction. These terms are proportional to C_2. In Figure 5, the coefficients, C_1 and C_2, are evaluated versus c_p/c_d, where c_p is the sound speed of a wave in the plate and c_d is the sound speed of a diffracted wave with wave number $\omega/c_d = \sqrt{k_s^2 k_l^2/(k_s^2 + k_l^2)}$. Near the sonic condition, edge diffraction dominates plate loading ($|C_2|$ is large). Above and below the sonic condition, both C_1 and C_2 are small. This represents the response at a resonance condition.

TABLE 1

Flexural plate wave material, electrical and geometric properties

SiN properties	Value	Electrical properties	Value
E	0·27 N/μm^2	B	$7{\cdot}78 \times 10^{-7}$ N/(A · μm)
ρ_p	$2{\cdot}95 \times 10^{-21}$ kg · m/μm^4	R	$7{\cdot}87 \times 10^{-3}$ Ω/(μm)
v	0·24		
Geometric properties	**Value**	**Air properties**	**Value**
L_x	2000 μm	B	$2{\cdot}14 \times 10^{-7}$ N/μm^2
h	1 μm	ρ	$1{\cdot}77 \times 10^{-24}$ kg · m/μm^4
		μ	$1{\cdot}85 \times 10^{-11}$ kg/μm · s

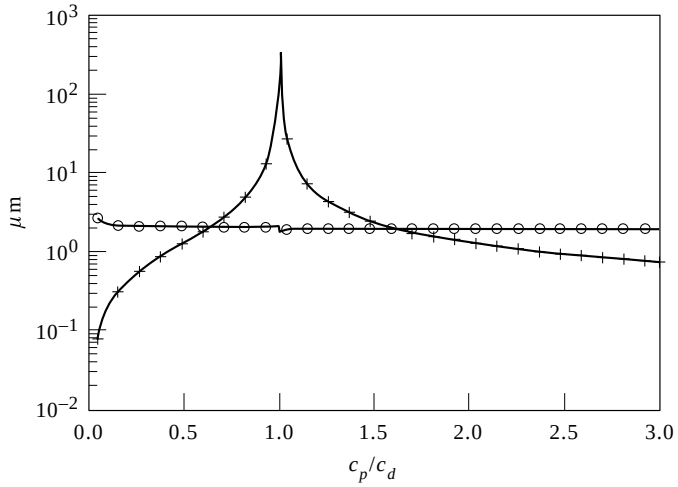

Figure 5. Relative contribution of response due to Wenzel's term and due to edge diffraction: ○, $|C_1|/(\rho\omega^2)$ terms; +, $|C_2|/(\rho\omega)^2$ terms.

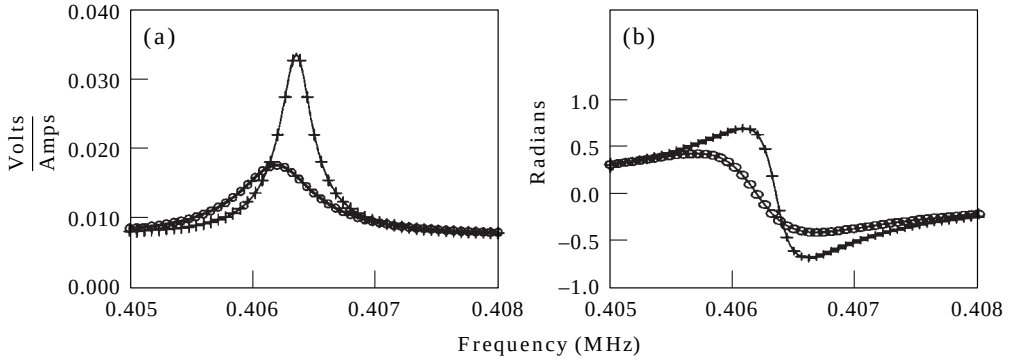

Figure 6. Calculated impedance of fluid loaded and unload sensor for subsonic waves in the plate, $c_p/c_d = 0{\cdot}336$; ○, with no fluid loading; +, with fluid loading. (a) Magnitude; (b) phase.

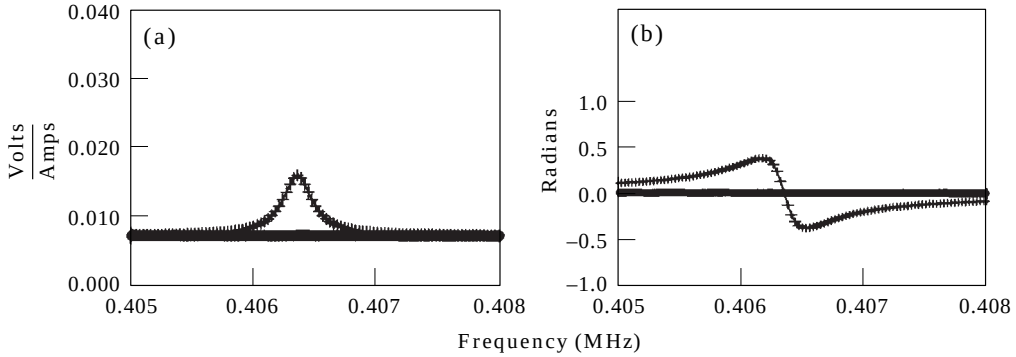

Figure 7. Calculated impedance of fluid loaded and unloaded sensor for sonic waves in the plate, $c_p/c_d = 1{\cdot}00$; ○, with no fluid loading; +, with fluid loading. (a) Magnitude; (b) phase.

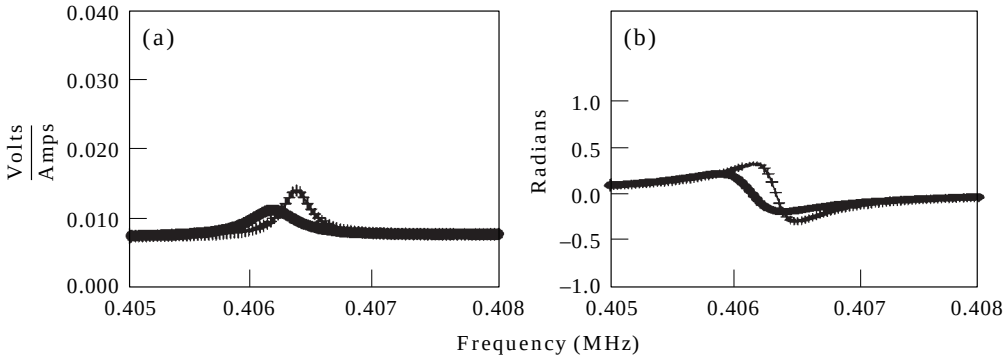

Figure 8. Calculated impedance of fluid loaded and unloaded sensor for supersonic waves in the plate, $c_p/c_d = 1{\cdot}34$; ○, with no fluid loading; +, with fluid loading. (a) Magnitude; (b) phase.

In Figures 6–8, the impedance (volts/amps) response of the fluid loaded FPW for subsonic, sonic, and supersonic waves in the plate is shown. Also shown in Figures 6–8 are the impedance responses of the FPW without fluid loading. If the viscosity of the fluid were zero in any condition, the fluid loaded and unloaded responses would be similar. Therefore, the dominant mechanism of damping in the fluid is not due to radiation but due to viscous relaxation. At the fluid/structure resonance, this loss is the greatest.

5. CONCLUSIONS

In this paper, a model representing the mechanisms of radiation and viscous relaxation in a fluid loaded Flexural Plate Wave (FPW) sensor has been presented. From this model it was determined that when the wave number of the FPW plate is close to the wave number of a diffracted surface wave, a fluid/structure resonance exists which produces substantial energy loss from the structure. This mechanism of viscous loss in MEMs devices has not been cited in the previous literature.

ACKNOWLEDGMENTS

I would like to thank Steven J. Martin, Gregory C. Frye, Daniel J. Segalman, Terry A. Michalski, and Julie A. Kesti for their insight and support of this work. Sandia is a multiprogram laboratory operated by Sandia Corporation, a Lockheed Martin Company, for the United States Department of Energy under Contract DE-AC04-94AL85000.

REFERENCES

1. D. J. Ballentine, S. J. Martin and A. J. Ricco 1996 *Acoustic Wave Sensors*: *Theory*, *Design & Physico-Chemical Applications*. San Diego, CA: Academic Press.
2. H. Hosaka, K. Itao and S. Kuroda 1995 *Sensors and Actuators*, *A Physical* **A49**, 87–95. Damping characteristics of beam-shaped micro-oscillators.

3. M. K. Andrews and P. D. Harris 1995 *Sensors and Actuators*, *A Physical* **A49**, 103–108. Damping and gas viscosity measurements using a microstructure.
4. K. Kokubun, M. Hirata, H. Murakami, Y. Toda and M. Ono 1984 *Vacuum* **34**, 731–735. A bending and stretching mode crystal oscillator as a friction vacuum gauge.
5. Z. Kadar, A. Bossche and J. Mollinger 1995 *Sensors and Actuators*, *A Physical* **A46–47**, 623–627. Design of a single-crystal silicon-based micromechanical resonator using finite element simulations.
6. Y.-H. Cho, B. M. Kwak, A. P. Pisano and R. T. Howe 1993 *Proceedings of Micro Electro Mechanical Systems*, 93–98. New York: IEEE. Viscous energy dissipation in laterally oscillating planar microstructures: a theoretical and experimental study.
7. S. W. Wenzel 1982 *Ph.D Thesis*, *Department of Electrical Engineering and Computer Sciences*, *University of California*, *Berkeley*, *CA*. Applications of ultrasonic lamb waves.
8. S. J. Martin, M. A. Butler, J. J. Spates, W. K. Schubert and M. A. Mitchell 1997 *Proceedings of the* 1997 *IEEE International Frequency Control Symposium*, 20–30. New York: IEEE. Magnetically-excited flexural plate wave resonator.
9. K. F. Graff 1975 *Wave Motion in Elastic Solids*. New York: Dover Publications.
10. L. Cremer, M. Heckl and E. E. Ungar 1988 *Structure-Borne Sound*; *Structural Vibrations and Sound Radiation at Audio Frequencies*. New York: Springer-Verlag.
11. S. Temkin 1981 *Elements of Acoustics*. New York: John Wiley.
12. M. Greenspan 1959 *Journal of the Acoustics Society of America* **32**, 70–73. Rotational relaxation in nitrogen, oxygen, and air.
13. J. D. Achenback 1987 *Wave Propagation in Elastic Solids*. New York: North-Holland.
14. G. F. Carrier, M. Krook and C. E. Pearson 1983 *Functions of a Complex Variable*; *Theory and Technique*. New York: McGraw-Hill.

APPENDIX: NOTATION

h	thickness of the plate
L_x	width of the plate
E	Young's modulus of plate material
v	Poisson's ratio of plate material
ρ_p	density of plate material
T	tension in the plate
$u_x(x)$, $u_y(x)$	displacement of the plate
i	current in wires
B	magnetic field
B	bulk modulus of fluid
μ_o	shear viscosity of fluid
μ_{v_o}	bulk viscosity of fluid
ρ	density of fluid
V_x	shear force in plate
M_x	moment in plate
τ_{xy}	shear stress in fluid
τ_{yy}	normal stress in fluid
$\theta = \partial u_y/\partial x$	rotation of plate
u_{y_1}	first perturbation of displacement
T_o, T_1	first perturbation of tension
M_{x_1}	first perturbation of moment
τ_{xy_1}, τ_{yy_1}	first perturbations of stresses
D	flexural rigidity

j	$= \sqrt{-1}$
ω	circular frequency
$\tilde{\phi}$	dilatational potential
$\tilde{\psi}$	shear potential
k_l	dilatational wave number
k_s	shear wave number
$\tilde{\Phi}$	wave number transform of dilatational potential
$\tilde{\Psi}$	wave number transform of shear potential
γ	wave number transform variable
q	$= \sqrt{k_l^2 - \gamma^2}$, $s = \sqrt{k_s^2 - \gamma^2}$
r	$= j\gamma h/2$
c_p	speed of sound in the plate
c_d	diffracted wave speed of sound in fluid
$x(\tilde{\omega})$	$= \int_{-\infty}^{\infty} x(t)\, e^{j\omega t}\, dt$ temporal Fourier transform
$X(\gamma)$	$= \int_{-\infty}^{\infty} x(x)\, e^{-j\gamma x}\, dt$ spatial Fourier transform